Space-time Estimation of Grid-cell Hourly Ozone Levels for Assessment of a Deterministic Model

Peter Guttorp **Wendy Meiring** **Paul D. Sampson**

NRCSE

Technical Report Series

NRCSE-TRS No. 007

Space-time estimation of grid-cell hourly ozone levels for assessment of a deterministic model

W. Meiring, P. Guttorp, and P.D. Sampson

Abstract

We present an approach to estimate hourly grid-cell surface ozone concentrations based on observations from point monitoring sites in space, for comparison with grid-based results from the SARMAP photochemical air-quality model for a region of Northern California. Statistical estimation is carried out on a transformed (square root) scale, followed by back-transforming to the original scale of ozone in parts per billion, adjusting for bias and variance. We estimate a spatially-varying diurnal mean structure and a non-separable space-time correlation structure on the transformed scale. Temporal prewhitening is followed by modeling of a spatially nonstationary, diurnally-varying spatial correlation structure using a spatial deformation approach. Comparisons of SARMAP model results with the estimated grid-cell ozone levels are presented.

Keywords: Kriging, Non-separable space-time correlation, Spatial scale, Transformation

1 Introduction

Photochemical air-quality models have been developed to better understand atmospheric pollutant levels and chemical reactions, and to predict the effects of regulated changes in pollutant emissions. The operational evaluation of such models consists of comparing model air quality predictions with any available observations. Observations may be obtained from various sources, including fixed surface monitoring sites, balloon-based instruments, and satellites. The results from the photochemical air-quality models are often on different spatial scales from the observations. Different processes manifest at different scales, as highlighted by the National Research Council (1991, page 305), which states "The spatial resolution of the concentrations predicted by a grid-based model corresponds to the size of the grid cell. Thus, effects that have spatial scale smaller than those of the grid cell cannot be resolved. Such effects include the depletion of ozone by reaction with nitric oxide (NO) near strong sources of NO_x like roadways and power plants." This quote highlights the need to consider the spatial scales of the model and observations in the model evaluation process. A grid-based numerical model has no information about variability on the subgrid scale, which is present in data from monitoring sites that are point locations in space. In this paper we present an approach to estimate hourly grid-cell surface ozone concentrations based on monitoring site observations, for comparison with grid-based predictions from the SARMAP photochemical air-quality model. We analyze data and model predictions from the Sacramento region and Northern San Joaquin Valley of California.

SARMAP stands for SJVAQS/AUSPEX Regional Model Adaptation Project; where

SJVAQS stands for San Joaquin Valley Air Quality Study; and AUSPEX stands for Atmospheric Utility Signatures, Predictions, and Experiments. As described in Blumenthal (1993), the SARMAP project aims included developing Eulerian models of atmospheric ozone and other pollutants in the San Joaquin Valley of California, to further develop the understanding of causes of ozone levels exceeding desirable limits, and to aid policy makers in deciding on emission control regulations. Extensive pollutant and meteorological data were collected at surface sites and for upper-air levels (including balloon-based and aircraft measurements) during the period July 1 through August 31, 1990 (Solomon and Silver, 1994). Intensive sampling periods were chosen to correspond with forecasted episodes of high ozone (Smith, 1994). Photochemical model results are available for the period August 3 through 6, 1990; which corresponds with an episode of high ozone. The SARMAP researchers have kindly provided us with the data and photochemical model output used here. In this paper we present analyses using only surface ozone data.

In order to estimate the grid-cell ozone concentrations, we begin by transforming the data to a scale where the residuals are approximately Gaussian. We then model a spatially varying diurnal (24 hour) mean structure and a spatially varying temporal correlation of the autoregressive type, which we use to pre-whiten the data. We use the spatial deformation approach developed by Sampson and Guttorp (1992) and Guttorp and Sampson (1994) to model the heterogeneous spatial correlation in the pre-whitened residuals, which also varies diurnally (Guttorp et al., 1994 and 1997). This spatial correlation model provides the basis for simple kriging estimates of the pre-whitened residuals at a regular sub-grid

of points in each grid cell for which the model produces results. We post-color the kriged residuals using autoregressive coefficients interpolated to the sub-grid points, and add back the diurnal mean field also interpolated to the sub-grid points. We then transform back to the original scale correcting for bias and variance due to the square-root transformation. This gives an estimate for the ozone level at each of the sub-grid points for each time point. Finally, we average the back-transformed values over all sub-grid points within each grid cell to give an estimate of the ozone concentration in parts per billion (ppb) for that grid cell. We also estimate the variance of this grid-scale estimate. Aspects of this analysis, namely the diurnal mean estimation, pre-whitening and spatial correlation estimation were presented in Guttorp et al. (1994, 1997).

Our approach represents a non-separable space-time correlation structure, in that the correlation cannot be expressed as a product of a spatial component and a temporal component. It allows for spatially varying mean fields, asymmetric estimates in space and time, and for diurnal variability in the correlation of the residuals. Diurnal variation in the spatial correlation structure has also been noted and attributed to geophysical processes by Casado et al. (1994), although these authors did not model a non-stationary spatial correlation structure. Non-stationarity and non-separability may be caused by complex influences of meteorology, topography, and emissions patterns on ozone levels. We are also investigating other non-separable space-time models (not based on temporal pre-whitening). See, for example, Sampson et al. (1994).

The approach we use for grid-cell estimation is essentially that described in section

3.2.2 of Cressie (1991), but in a spatio-temporal context with temporal pre-whitening and a diurnal mean structure. Cressie suggests transforming the data to a scale where they are approximately Gaussian, performing kriging on the transformed scale, and then correcting for bias when transforming back to the original scale. He gives details for the log transform, and generalizes it for other transformations. The transformation and pre-whitening steps in our approach make the usual block kriging calculations (c.f., Journel and Huijbregts, 1978; Cressie, 1991, page 124) infeasible, which is why we estimate at a regular sub-grid of points before averaging.

An outline of the remainder of the paper is as follows. In section 2, we present the spatio-temporal modeling approach (Guttorp et al., 1994 and 1997). Section 3 provides more details of the grid cell estimation, referring to Appendices A and B for expressions for the moments of the spatio-temporal process as well as implementation of a forward recursion estimation approach for grid cell ozone levels. Several other practical implementation issues are discussed in section 4. In section 5, we present estimates of the surface ozone levels with standard errors for several grid cells in the Sacramento region and Northern San Joaquin Valley, under the assumption of known mean and covariance structure. We compare these with results from the SARMAP photochemical air-quality model. We conclude with a discussion indicating directions for future work.

2 The data

Figure 1 shows a map of California with 32 of the SARMAP surface ozone sites indicated by open circles. These are the 32 sites used in Guttorp et al. (1997). Site descriptions of a subset of these sites are provided in Guttorp et al. (1994), which also discusses the exclusion of one site in this region due to data quality problems. The enlarged subpanel also indicates the centers of the SARMAP photochemical model grid cells. The positions of a sub-grid of nine points in one grid cell are also shown, and will be discussed in section 5.

... Figure 1 about here ...

There is extreme heterogeneity of variance in the hourly ozone data, with means and variances positively related. After considering several transformations of the data, we used the square root transformation. Carroll et al. (1997) also chose a square root transform for analyzing surface ozone data.

Figures in Guttorp et al. (1994, 1997) indicated a strong diurnal cycle in mean ozone levels at each site, usually with a maximum in the afternoon in this region. Ozone is a secondary pollutant produced in photochemical reactions (c.f., NRC, 1991). Diurnal patterns in photochemical activity, primary pollutant emission and pollutant transport explain the diurnal structure. Peaks in the diurnal cycle of surface ozone may occur at different hours at different sites due to the transport of pollutants. We estimated and subtracted site-specific hourly means on the square root scale. These were later interpolated for grid cell estimation. Figure 2 contains contour maps of the site-specific means of the

data at hours 2, 7, 15 and 20. These illustrate that the diurnal mean structure is spatially varying.

... **Figure 2 about here** ...

2.1 Temporal correlation

Autocorrelation plots presented in Guttorp et al. (1994) showed very strong temporal correlation in the residuals after removing a diurnal mean structure. As described there, we used site-specific autoregressive filters of order 2, AR(2) models, to temporally pre-whiten the residuals after removing hourly means. Parameter estimation used Gaussian maximum likelihood.

We chose AR(2) as parsimonious models filtering out most of the short-range temporal correlation. More complex models such as periodic autoregressive models and seasonal ARIMA models could be used as pre-whitening filters. Periodic autoregressive models would allow a diurnally varying temporal correlation structure, explained by the diurnal cycle in the production, accumulation and depletion of ozone (Tiao and Grupe, 1980). Seasonal ARIMA models could better model residual 24 hour lag correlation (c.f., Box et al., 1994, section 9.1). One could easily extend the grid cell level estimation approach presented here to periodic autoregressive models (c.f., section 4). The extension to seasonal ARIMA filters would require substantially more complex cross-product moment estimates than those presented in Appendix A.

Figure 3 indicates the relative magnitudes of the AR(2) coefficients for each site. An arrow originates at each of the site locations. The horizontal length of each arrow is pro-

portional to the magnitude of the lag 1 coefficient of the AR(2) model, while the vertical length is proportional to the magnitude of the lag 2 coefficient in the AR(2) model. The arrows vary smoothly in space.

... **Figure 3 about here** ...

2.2 Spatial correlation in pre-whitened ozone residuals

Given data $\{z_t(x_i) \mid i = 1, \ldots N, t = 1, \ldots, T\}$, for N monitoring sites and T time points, let $v_t(x_i) = \sqrt{z_t(x_i)}$. Let $h_t(x_i)$ denote the mean of the ozone levels on the square root scale at site x_i for the hour of day corresponding to time t, and let $w_t(x_i) = v_t(x_i) - h_t(x_i)$. We express

$$w_t(x_i) \quad = \quad \alpha_1(x_i)\, w_{t-1}(x_i) + \alpha_2(x_i)\, w_{t-2}(x_i) + y_t(x_i)$$

where $y_t(x_i)$ is the pre-whitened residual at site x_i.

We assume that $y_t(x_i)$, $i \in \{1, \cdots, N\}$, $t \in \{1, \cdots, T\}$ is a sample from a diurnally varying space-time process $\{Y_t(x)\}$ which is uncorrelated in time, but correlated in space. We also assume that $Y_t(w) = U_t(w) + \epsilon_t(w)$ where the spatial correlation between $U_t(w)$ and $U_t(u)$ is a smooth function of geographic location for all sites w and u, and where $\epsilon_t(x)$ represents spatially and temporally independent measurement error. We assume that $D_t(u, w)$, the spatial dispersion on the standardized scale between sites u and w at time t satisfies

$$D_t(u,w) \quad \stackrel{\text{def}}{=} \quad \text{Variance}\left(\frac{Y_t(u)}{\sqrt{Y_t(u)}} - \frac{Y_t(w)}{\sqrt{Y_t(w)}}\right) \to a_t \quad \text{as} \quad \| u - w \| \to 0$$

where a_t is known as the nugget effect at time t. In practice we cannot distinguish between small-scale variability and measurement error, since we do not have collocated monitoring instruments. Both of these components are included in the estimated nugget effect. In this analysis, we have estimated a constant variance field in space. The variance field varies with hour of day.

Guttorp et al. (1994) indicated that the fitted spatial correlation structure of the pre-whitened residuals for 17 sites in the Sacramento region varied with time of day, being weaker and more homogeneous in the morning hours 0 through 4 am, than during the afternoon hours noon through 4 pm. Guttorp et al. (1997) illustrated that the spatial correlation of the prewhitened residuals also varies with hour of day for the larger region of 32 sites.

If time points t_1 and t_2 correspond to the same hour of day, then we assume that $D_{t_1}(u,w) = D_{t_2}(u,w)$ for any pair of sites u and w. We also assume that the time slices of pre-whitened residuals from the same hour of day are independent spatial samples from the process $\{Y_t(w)\}$ at this hour of day, giving us replications to use in estimating the spatial correlation for each hour. The heterogeneous spatial correlation estimation procedure developed by Sampson and Guttorp (1992) and Guttorp and Sampson (1994) makes use of such replications, and we apply their estimation approach for each hour of the day. The sample dispersion between monitoring sites x_i and x_j at hour k is estimated as $d_{ijk} = 2\,(1 - r_{ijk})$ where r_{ijk} is the sample correlation between the observations at sites x_i and x_j at hour k.

The spatial dispersion model between sites u and w at hour k is

$$D_k(u,w) \quad = \quad \gamma_{\theta_k}\left(\parallel g_k(u) - g_k(w) \parallel\right)$$

where γ_{θ_k} is an isotropic variogram model with parameters θ_k, $\parallel \ . \ \parallel$ denotes euclidean distance, and g_k is a bijective mapping from $\Re^2$ to $\Re^2$. In other words the spatial dispersion is modeled by an isotropic variogram as a function of distance in a deformed plane, known as the D-plane. Each mapping g_k consists of two $\Re^2 \rightarrow \Re$ thin-plate spline mappings as described in Sampson and Guttorp (1992) and Guttorp et al. (1994). The D-plane variogram model γ_{θ_k} must be chosen, and the parameters and the deformation must be estimated. In this study we use an exponential variogram model for the isotropic D-plane variogram. It is of the form

$$\gamma_{(a_k,t_k)}(r) \quad = \quad \begin{cases} a_k + (2 - a_k)\left\{1 - \exp\left(-t_k r\right)\right\} & \text{if } r > 0 \\ 0 & \text{otherwise} \end{cases} \qquad (1)$$

for hour k and sites a distance r apart. The parameter a_k is the nugget effect (between 0 and 2), and t_k controls the rate of increase of the variogram ($t_k > 0$). This variogram is monotonically increasing and approaches 2, corresponding to zero correlation, as the distance between sites increases. Substitution of $\parallel g_k(u) - g_k(w) \parallel$ for r in equation (1) gives the model as a function of geographic location for sites u and w.

Once the isotropic D-plane variogram model has been chosen, the variogram parameters and the D-plane locations corresponding to the monitoring sites are estimated by minimizing a penalized weighted least squares criterion between the fitted and the sample dispersions. The penalty is on the degree of bending of the mapping from the geographic plane to the

D-plane. Specifically the criterion is

$$C_{\theta_k,g_k,\lambda} = \sum_{j=2}^{N}\sum_{i=1}^{j-1}\left[\frac{d_{ijk}-\widehat{d_{ijk}}}{\widehat{d_{ijk}}}\right]^2 + \lambda\ \mathrm{BEP_k}, \tag{2}$$

where $\widehat{d_{ijk}}$ is the fitted dispersion between sites x_i and x_j at hour k, BEP_k is the bending energy penalty computed as the sum of the bending energies of the two thin-plate splines for hour k, and λ is a smoothness parameter. For small values of λ, we may get overfitting of the sample dispersions and a mapping that folds. The mapping will approach an affine mapping for large λ. Cross-validation may be used to choose the value of λ (c.f., Meiring et al., 1997). The D-plane coordinates resulting from minimization of (2) determine a pair of interpolating thin-plate splines for the mappings of the geographic coordinates to the deformed coordinates for each hour. These thin-plate spline mappings allow estimation of the spatial correlation between any two geographic locations. Due to computational magnitude, we did not use cross-validation in this study. Visual inspection of the fitted variograms versus D-plane distances and deformation maps was used to choose a single value of λ for all hours.

3 Estimation of grid cell ozone levels

We now present details of the grid cell estimation approach. Let $Z_t(w)$ denote the ozone level at location w and time t, and let $V_t(w) = \sqrt{Z_t(w)}$ denote the square root of the ozone level. Let $h_t(x)$ denote the mean of the ozone levels on the square root scale at site x for the hour of day corresponding to time t. The pre-whitening filter is a function of time and

spatial location:

$$V_t(w) = W_t(w) + h_t(w) \tag{3}$$

$$W_t(w) = \alpha_1(w)W_{t-1}(w) + \alpha_2(w)W_{t-2}(w) + Y_t(w) \tag{4}$$

where $\alpha_1(w)$ and $\alpha_2(w)$ are site-specific AR(2) coefficients, and $Y_t(w)$ is the residual process at location w and time t. For notational convenience, define

$$\mathcal{Y}_t \equiv \{Y_t(x_1) = y_t(x_1), \ldots, Y_t(x_N) = y_t(x_N),\ \mathcal{Y}_{t-1}\}.$$

We assume that $Y_t(w)$ is independent of everything that happened prior to time t, for any site w and time t. The estimation of the grid cell ozone levels and variability of these levels is accomplished using a forward recursive estimation of moments given in Appendix A. The forward recursion is described briefly in Appendix B.

For simplicity we only describe here the estimation for one model grid cell, denoted A. We choose M regularly spaced (sub-grid) points in A, denoted by $w_1, \ldots, w_M$. Using the approach described in section 2.2, we evaluate the fitted covariances $\mathrm{cov}(Y_t(w_i), Y_t(w_j))$, $\mathrm{cov}(Y_t(w_i), Y_t(x_k))$, and $\mathrm{cov}(Y_t(x_l), Y_t(x_k))$ for all sub-grid points w_i and w_j in block A, and all monitoring sites x_k and x_l. We interpolate the AR(2) pre-whitening coefficients and diurnal mean structure to each of the M points (c.f., section 4.1).

At each of the M sub-grid points, we estimate the simple kriging mean $E[Y_t(w_i)|\ \mathcal{Y}_t]$ and variance $\mathrm{Var}[Y_t(w_i)|\ \mathcal{Y}_t]$ of the pre-whitened residuals, assuming $\{Y_t(w)\}$ is a zero mean process. We also estimate other moments of the residuals, including cross-product moments, which are needed when back-transforming to estimate ozone concentrations and

assess variability on the original scale (ozone in ppb), as described in Appendix A. At each grid point, we post-color the kriged pre-whitened residuals (c.f. Appendix A), using the interpolated AR(2) coefficients, and add the interpolated hourly mean corresponding to each time point to the post-colored values. We back-transform to the original scale of ozone in ppb, adjusting for bias, and estimate the grid cell level

$$\frac{1}{\mid A \mid} \int_A V_t(w)^2 \, dx \qquad \text{by} \qquad \frac{1}{M} \sum_{j=1}^{M} E \left[\, V_t(w_j)^2 \;\mid\; \mathcal{Y}_t \, \right], \tag{5}$$

which is different from the average of the squares of the estimates on the square root scale.

We estimate the variability of this grid cell estimate as

$$\begin{aligned} &\text{Var} \left[\frac{1}{M} \sum_{j=1}^{M} \left[\, V_t(w_j)^2 \;\mid\; \mathcal{Y}_t \, \right] \right] \\ &= \frac{1}{M^2} \left(\sum_{j=1}^{M} \text{Var} \left[\, V_t(w_j)^2 \;\mid\; \mathcal{Y}_t \, \right] + 2 \sum_{i<j} \text{Cov} \left[V_t(w_j)^2 \, , \; V_t(w_i)^2 \;\mid\; \mathcal{Y}_t \, \right] \right). \end{aligned} \tag{6}$$

The estimates in equations (5) and (6) could be modified to accommodate a spatially-varying variance field, by including weights in the estimates. In this study we have estimated a constant variance field for the entire region, although this could also easily be modified.

This estimate of variability assumes that both the mean and covariance structure of the random function in space and time are known, and thus underestimates the true variability. It does not take into account variability from estimating the covariance or interpolating the mean field and the AR(2) coefficients. Extensions to more accurate estimates of the variability are indicated in section 6.

4 Implementation issues

In this section we discuss the interpolation of the AR(2) coefficients and of the diurnal mean structure, practical issues in the spatial correlation estimation approach, and the impact of missing data on the estimation. The forward recursion estimation approach is described in Appendices A (moment expressions) and B (computational implementation).

4.1 Interpolation of the autoregressive parameters and mean field

When interpolating the autoregressive parameters to the regular grid points for grid cell estimation, we need to constrain the interpolation to give stationary autoregressive models, i.e., we require

$$1 - \alpha_1(w) - \alpha_2(w) \;>\; 0, \qquad 1 - \alpha_2(w) + \alpha_1(w) > 0, \quad \text{and} \quad |\alpha_2(w)| < 1$$

for all monitoring sites and interpolation points w (c.f., Kendall and Ord, 1990, page 59). Jones (1980) suggests a reparameterization approach for ensuring that the stationarity constraints are satisfied for ARMA(p, q) processes in a non-linear optimization problem. This reparameterization allows us to interpolate subject to the stationarity constraints. For our simple case of the AR(2) model, let $\phi_1(w)$ and $\phi_2(w)$ denote the partial autoregressive coefficients at site w, and define

$$\beta_i(w) \;=\; \log\left[\frac{1+\phi_i(w)}{1-\phi_i(w)}\right]. \qquad \text{This gives} \qquad \phi_i(w) = \left[\frac{1-\exp\left(-\beta_i(w)\right)}{1+\exp\left(-\beta_i(w)\right)}\right],$$

so $\phi_i(w) \in (-1, 1)$, for $i = 1, 2$. By interpolating $\{\beta_i(x_i), i \in 1, \ldots, N\}$ instead of the autoregressive coefficients directly, to each of $w_1, \ldots, w_M$, we ensure stationarity of the

autoregressive coefficients. The autoregressive coefficients are then calculated as

$$\alpha_1(w_j) = \phi_1(w_j)(1-\alpha_2(w_j)) \qquad \text{and} \qquad \alpha_2(w_j) = \phi_2(w_j).$$

We interpolated using the Splus function *interp* (Statistical Sciences, 1991) within the convex hull of the monitoring sites. This function is based on the work of Akima (1978). We also used this approach to interpolate the diurnal mean field.

The forward recursive moments presented in section 3 and Appendix A could easily be modified to use periodic autoregressive models as the prewhitening models. The only change would be to replace $\alpha_j(x)$ by $\alpha_{jk}(x)$ for hour k where appropriate, taking care to use the correct time lag in the pre-whitening coefficients. The stationarity constraints would be more complex however.

4.2 Spatial correlation estimation

Due to the short time series of two months of hourly observations, we actually base the sample dispersion estimates for each hour and each pair of sites on a three hour window of residuals centered at the specified hour (i.e., $3 \times 62 = 186$ residuals if there are no missing data), weighted equally. We then model the spatial correlation of these pre-whitened residuals separately for each three hour window of residuals. That is we estimate 24 deformation and D-plane variogram models, each based on three hours of residuals, giving a smoothly varying diurnal cycle in the spatial correlation structure. There is thus two hours of overlap in the sample dispersion estimates for adjacent hours. Plots in Guttorp et al. (1997) indicate that the large scale features of the spatial correlation in the afternoon hours remain

relatively similar, even for the deformations based on non-overlapping sets of hours.

In the early morning the pairwise correlations are low, so the deformation structure does not have a clear interpretation. Estimation of the deformation structure becomes very difficult in the morning hours, since the estimation procedure cannot distinguish between a variogram with a high nugget and relatively flat slope, or one with a very low nugget and a steep rise before distances where data are available. The correlation structure becomes stronger in the afternoon hours, and the deformation becomes more meaningful. Estimation of the nugget is still difficult, since we have no information at distances less than the smallest inter-site distance. We fitted a relatively large nugget for each hour, so the estimated measurement error and small scale variability is large. Figure 4 shows the deformation mapping and fitted dispersions as a function of D-plane distance for 4 pm in the afternoon.

... **Figure 4 about here** ...

4.3 Missing values

At each time point t, all the prewhitened residuals that are available at that time point are used in the estimation. The kriging weights vary with hour of day, and with the pattern of non-missing observations. Missing values present no problem in iterating forward in time; however, they may cause substantial biases in estimates of the diurnal mean structure, the AR(2) coefficients, and the spatial correlation. The observations are often not missing at random, since sites were operational at different times. A few sites in this region either have no observations for hour 4, or for hour 5. If a site were missing all the observations at one of these hours, the mean for that hour was estimated as the average of the means for

the two neighboring hours. Further study is needed on the impact of missing values.

5 Application: Grid-cell estimation for a region of California

SARMAP photochemical air-quality model results were available for the period August 3 through August 6, 1990. We estimated hourly grid cell ozone levels for each of 76 grid cells corresponding to grid cells of the photochemical air quality model in the region of California indicated by figure 1. The estimate in each grid cell is based on nine regularly spaced locations in the grid cell, with four of them corresponding to the corners of the grid cell.

The top plot of figure 5 shows the estimated grid cell ozone concentration, $\pm$ two standard errors, and the SARMAP photochemical air-quality model concentrations for a single grid cell ($i = 11$, $j = 36$) on the days when we had photochemical model results. The nine sub-grid points for this grid cell are shown by crosses in figure 1. The lower plot of figure 5 shows time series of ozone records at three monitoring sites which are in or nearby the grid cell. These three sites are partially covered by the crosses in figure 1.

The SARMAP model output shown here is more recent than that available for Meiring (1995), and represents a substantial improvement in the model results for this grid cell, with better representation of the diurnal cycle and peaks of the grid cell concentration. There is overestimation of ozone levels during the night and early morning hours, but the peaks agree quite well.

... **Figure 5 about here** ...

Appendix A provides formulae for point and grid-cell estimation, as well as for back-transforming to the original scale of ppb. Figure 6 shows the estimated variance of the back-transformed point estimate at the central sub-grid point of this grid-cell (horizontal axis), compared with the estimated variance of the grid-cell estimate in ppb (vertical axis). The estimated variance of the grid-cell estimate is substantially smaller than that of the point estimate.

... **Figure 6 about here** ...

Figures 7 and 8 contain image plots of the grid cell estimates and the estimated variances, together with the photochemical air quality model results, and the difference between the air quality model results and the estimated ozone levels, for each of hours 2 and 16 of August 4, 1990. Four of the planned 80 grid cells lack estimates due to extrapolation problems outside the convex hull of the 32 sites. At hour 2 we observe that the photochemical model results are higher than our estimated ozone levels. This is consistent with the patterns during the early morning hours for the other days during this four day period. At hour 16 of August 4, some grid cell model results are higher than our estimates, while others are lower. Figure 8 shows regions where the model and grid cell estimates disagree substantially on this day and time, including the south-western part of this region.

... **Figure 7 about here** ...

... **Figure 8 about here** ...

Due to space limitations, we can unfortunately not provide image plots for other dates and times of day, or time series comparisons for more grid cells. A detailed evaluation of

the model would require these.

6 Discussion

Carroll et al. (1997) present an alternative approach for estimating ozone levels and conditional covariances at different sites and times on the original scale, while doing their modeling on a (shifted) square root scale. They use a stationary space-time covariance structure in their estimation, and assume a known temporal trend. By contrast, we use a temporal pre-whitening approach after removing a diurnal mean structure, and then use heterogeneous spatial covariance estimates for the pre-whitened residuals as the covariance in the kriging equations when estimating at an unmonitored site. We assumed the diurnal mean structure to be known in this initial work, but some variability in a temporal "trend" K_{wt} is still included through the moments of K_{wt} given in Appendix A.

Huang and Cressie (1996) developed a space-time Kalman filter with AR(p) temporal models with constant coefficients in space. In many respects our space-time model on the transformed scale is similar to that of Huang and Cressie (1996). Notable differences are that we use a fixed diurnally varying spatial covariance structure whereas theirs is updated in the Kalman filter recursions. We have spatially varying autoregressive parameters and we use simple kriging since we assume the mean of the residual process is zero. The space-time Kalman filter of Wikle and Cressie (1996) explicitly models space-time lags in the correlation, which may help to statistically model transport of pollutants. We do not model space-time lagged correlation through a single space-time correlation model, however the

moments of the W process are not necessarily symmetric in space and time due to the diurnal cycle in the spatial covariances and the spatial dependence of the autoregressive coefficients. Patterns of transport of ozone and of ozone precursors from one site to another will mainly be captured through differences in the hourly mean ozone structure at different sites in our model. Peaks of the ozone cycle may occur at different hours at different sites. Our spatial correlation structure varies with hour of day and the temporal correlation varies in space, yielding a non-separable space-time correlation structure.

A non-parametric bootstrap could be used to assess the additional variability in the block estimates due to estimation of the spatial covariances. This approach would involve bootstrapping spatial realizations (time slices) from the prewhitened residuals, followed by estimation of the spatial correlation structure based on each of these bootstrap samples as described in Meiring (1995), and estimating grid cell levels using the spatial correlation structure for each bootstrap sample. This approach is computationally intensive. We need to work further on computational algorithms and methods to handle missing values to make this bootstrap evaluation feasible in practice. A parametric bootstrap approach as presented in Guttorp et al. (1993b), or kriging (see Høst et al., 1995), could be used to assess additional variability due to estimation of the mean field and of the pre-whitening coefficients.

An alternative approach is through a Bayesian formulation which would allow uncertainty in the parameters of the autoregressive models and diurnal mean structure. Prior distributions could include spatial correlation amongst these parameters. We currently

take the spatial correlation into account through smoothing. Implementation of the heterogeneous spatial correlation estimation approach of section 2.2 in a Bayesian framework remains as future work. One approach for directly integrating our empirical spatial correlation estimates in a Bayesian framework has been demonstrated in Guttorp et al. (1993a) and Brown et al. (1994). There are many other areas of future work for the spatial correlation estimation approach, including how best to constrain the deformation mappings to be bijective, since the thin-plate splines do not impose this constraint, although it may be obtained by choosing λ sufficiently large in (2).

It will be useful to view the evolution of the estimated grid-cell ozone levels in space and time for comparison with the evolution of the model results in space and time. The geophysical model is a numerical approximation to reality, based on simplified physics, so one would not expect the data and model results to agree exactly. Comparisons of the type described in this paper may indicate systematic or large-scale deviations between the geophysical model and data, and specific aspects of the model which require further improvement.

A Appendix: Moments

We now describe the estimation of the terms in equations (5) and (6) in more detail. Let

$$K_{wt} = \alpha_1(w)W_{t-1}(w) + \alpha_2(w)W_{t-2}(w) + h_t(w), \tag{7}$$

with $W_t(w)$, $\alpha_1(w)$, $\alpha_2(w)$ and $h_t(w)$ as defined in equations (3) and (4). It follows that the expected ozone level at site location w, conditional on the monitoring site data up to

and including time t, is given by

$$\begin{aligned} E\left[Z_t(w) \mid \mathcal{Y}_t\right] &= E\left[V_t(w)^2 \mid \mathcal{Y}_t\right] \\ &= E\left[(K_{wt} + Y_t(w))^2 \mid \mathcal{Y}_t\right] \\ &= E\left[K_{wt}^2 \mid \mathcal{Y}_t\right] + 2E\left[K_{wt} \mid \mathcal{Y}_t\right] E\left[Y_t(w) \mid \mathcal{Y}_t\right] + E\left[Y_t(w)^2 \mid \mathcal{Y}_t\right]. \end{aligned}$$

We thus need to estimate the conditional moments of $Y_t(w)$ and K_{wt} up to order two for estimation of ozone at each grid point location. In order to estimate the variance (equation 6) of the average of the point estimates (equation 5), we also need the conditional moments and cross-product moments up to order four, since equations (3), (4) and (7) imply that

$$\begin{aligned} V_t(w)^4 &= K_{wt}^4 + 4K_{wt}^3\, Y_t(w) + 6K_{wt}^2\, Y_t(w)^2 + 4K_{wt}\, Y_t(w)^3 + Y_t(w)^4 \\ V_t(w)^2 V_t(u)^2 &= \left(K_{wt}^2 + 2K_{wt}\, Y_t(w) + Y_t(w)^2\right)\left(K_{ut}^2 + 2K_{ut}\, Y_t(u) + Y_t(u)^2\right) \\ &= K_{wt}^2 K_{ut}^2 + 2K_{wt}^2 K_{ut}\, Y_t(u) + K_{wt}^2\, Y_t(u)^2 + 2K_{wt}K_{ut}^2\, Y_t(w) \\ &\quad + 4K_{wt}K_{ut}\, Y_t(w)\, Y_t(u) + 2K_{wt}\, Y_t(w)\, Y_t(u)^2 + K_{ut}^2\, Y_t(w)^2 \\ &\quad + 2K_{ut}\, Y_t(u)\, Y_t(w)^2 + Y_t(w)^2\, Y_t(u)^2 \end{aligned}$$

Expressions for the conditional moments in equations (5) and (6) as functions of conditional moments and cross-product moments of the residual field follow by taking conditional expectations of the previous expressions. We discuss estimation of the residual field moments in sections A.1 and A.2, and of moments involving K_{wt} in section A.3.

A.1 Estimation of the residual field at any location

If $Y_t(w)$ is the pre-whitened residual at a spatial location w, and if we assume that

$$Y_t(w), Y_t(x_1), \ldots, Y_t(x_N) \quad \sim \quad \mathrm{N}_{N+1}\left(0, \begin{bmatrix} \sigma_{ww}(t) & \Sigma_{w2}(t) \\ \Sigma_{2w}(t) & \Sigma_{22}(t) \end{bmatrix}\right),$$

where $\Sigma_{w2}(t)$ is $1 \times N$, $\Sigma_{2w}(t)$ is $N \times 1$ and $\Sigma_{22}(t)$ is $N \times N$, then

$$Y_t(w) \mid \mathcal{Y}_t \quad \sim \quad \mathrm{N}_1\left(\theta_{wt}, \sigma^2_{wt}\right)$$

where

$$\theta_{wt} \quad = \quad \Sigma_{w2}(t)\Sigma_{22}(t)^{-1} \begin{bmatrix} y_t(x_1) \\ \vdots \\ y_t(x_N) \end{bmatrix} \qquad \text{and} \qquad \sigma^2_{wt} = \sigma_{ww}(t) - \Sigma_{w2}(t)\Sigma_{22}(t)^{-1}\Sigma_{2w}(t),$$

and $\sigma_{ww}(t)$, $\Sigma_{w2}(t)$ and $\Sigma_{2w}(t)$ depend on w and t. θ_{wt} and σ^2_{wt} are simple kriging means and variances. Simple kriging provides the best linear estimator of the value at a site conditional on records from monitoring sites, assuming known mean and spatial covariance structure. The estimator is 'best' in terms of squared error loss. We can estimate the correlation between any two sites using the deformation model, and hence (after interpolating the variance field, since Σ is a covariance matrix) estimate θ_{wt} and σ^2_{wt} at any location. Equations (8), (9), and (10) follow from theory of the Gaussian distribution:

$$E\left[Y_t(w)^2 \mid \mathcal{Y}_t\right] \quad = \quad \sigma^2_{wt} + \theta^2_{wt} \tag{8}$$

$$E\left[Y_t(w)^3 \mid \mathcal{Y}_t\right] \quad = \quad 3\theta_{wt}\sigma^2_{wt} + \theta^3_{wt} \tag{9}$$

$$E\left[Y_t(w)^4 \mid \mathcal{Y}_t\right] \quad = \quad 3\sigma^4_{wt} + 6\sigma^2_{wt}\theta^2_{wt} + \theta^4_{wt}. \tag{10}$$

A.2 Pairwise cross-product moments between residuals

Consider two locations, w and u, in a grid cell A. If we assume that

$$Y_t(u), Y_t(w), Y_t(x_1), \ldots, Y_t(x_N) \sim \mathrm{N}_{N+2}\left(0, \begin{bmatrix} \sigma_{uu}(t) & \sigma_{uw}(t) & \Sigma_{u2}(t) \\ \sigma_{wu}(t) & \sigma_{ww}(t) & \Sigma_{w2}(t) \\ \Sigma_{2u}(t) & \Sigma_{2w}(t) & \Sigma_{22}(t) \end{bmatrix}\right),$$

then

$$Y_t(u) \mid Y_t(w), Y_t(x_1), \ldots, Y_t(x_N) \sim \mathrm{N}\left(\alpha_{u|w}(t), \eta^2_{u|w}(t)\right)$$

where

$$\alpha_{u|w}(t) = \begin{bmatrix} \sigma_{wu}(t) & \Sigma_{2u}(t) \end{bmatrix} \begin{bmatrix} \sigma_{ww}(t) & \Sigma_{w2}(t) \\ \Sigma_{2w}(t) & \Sigma_{22}(t) \end{bmatrix}^{-1} \begin{bmatrix} Y_t(w) \\ y_t(x_1) \\ \vdots \\ y_t(x_N) \end{bmatrix}$$

$$\eta^2_{u|w}(t) = \sigma_{uu}(t) - \begin{bmatrix} \sigma_{wu}(t) & \Sigma_{2u}(t) \end{bmatrix} \begin{bmatrix} \sigma_{ww}(t) & \Sigma_{w2}(t) \\ \Sigma_{2w}(t) & \Sigma_{22}(t) \end{bmatrix}^{-1} \begin{bmatrix} \sigma_{uw}(t) \\ \Sigma_{u2}(t) \end{bmatrix}.$$

It follows that

$$E\left[Y_t(u)^2 \mid Y_t(w), \ \mathcal{Y}_t \right] = \eta^2_{u|w}(t) + \alpha^2_{u|w}(t)$$

Both $\eta_{u|w}(t)$ and $\alpha_{u|w}(t)$ depend on w and u through the covariance $\sigma_{wu}(t)$, but only $\alpha_{u|w}(t)$ depends on $Y_t(w)$. $\alpha_{u|w}(t)$ may be written as

$$\alpha_{u|w}(t) = a_{u|w}(t)\, Y_t(w) + c_{u|w}(t),$$

$$\text{so} \qquad \alpha^2_{u|w}(t) \;=\; a^2_{u|w}(t) Y_t(w)^2 + 2a_{u|w}(t)c_{u|w}(t)\; Y_t(w) + c^2_{u|w}(t).$$

It follows that

$$\begin{aligned} E\left[\; Y_t(w)^2\; Y_t(u)^2 \mid \; \mathcal{Y}_t \;\right] &= E\left(\; Y_t(w)^2 \;\; E\left[\; Y_t(u)^2 \mid Y_t(w), \;\; \mathcal{Y}_t \;\right] \;\mid\; \mathcal{Y}_t \;\right) \\ &= \left(\eta^2_{u|w}(t) + c^2_{u|w}(t)\right) E\left[Y_t(w)^2 \mid \mathcal{Y}_t\right] + a^2_{u|w}(t) E\left[Y_t(w)^4 \mid \mathcal{Y}_t\right] + \\ &\quad 2a_{u|w}(t)c_{u|w}(t) E\left[Y_t(w)^3 \mid \mathcal{Y}_t\right], \end{aligned}$$

$$\begin{aligned} E\left[\; Y_t(w)\; Y_t(u) \mid \mathcal{Y}_t\right] &= E\left[\; Y_t(w) E\left[\; Y_t(u) \mid Y_t(w), \; \mathcal{Y}_t\right] \;\mid\; \mathcal{Y}_t\right] \\ &= a_{u|w}(t) E\left[Y_t(w)^2 \mid \mathcal{Y}_t\right] + c_{u|w}(t) E\left[Y_t(w) \mid \mathcal{Y}_t\right], \qquad \text{and} \end{aligned}$$

$$\begin{aligned} E\left[\; Y_t(u)\; Y_t(w)^2 \mid \mathcal{Y}_t\right] &= E\left[\; Y_t(w)^2 E\left[\; Y_t(u) \mid Y_t(w), \; \mathcal{Y}_t\right] \;\mid\; \mathcal{Y}_t\right] \\ &= a_{u|w}(t) E\left[Y_t(w)^3 \mid \mathcal{Y}_t\right] + c_{u|w}(t) E\left[Y_t(w)^2 \mid \mathcal{Y}_t\right]. \end{aligned}$$

A.3 Other Moments

The moments of K_{wt} involve recursive moments of $W_t(w)$, which we estimate at each time point, based on prior estimates. We present the formulae for K_{wt}, followed by the formulae for the moments of $W_t(w)$. It is immediate from equation 7 that

$$\begin{aligned} E\left[K_{wt} \mid \mathcal{Y}_t\right] &= \alpha_1(w) E\left[W_{t-1}(w) \mid \mathcal{Y}_t\right] + \; \alpha_2(w) E\left[W_{t-2}(w) \mid \mathcal{Y}_t\right] + h_t(w) \\ E\left[K^2_{wt} \mid \mathcal{Y}_t\right] &= \alpha_1(w)^2 E\left[W_{t-1}(w)^2 \mid \mathcal{Y}_t\right] + 2\; \alpha_1(w)\; \alpha_2(w) E\left[W_{t-1}(w) W_{t-2}(w) \mid \mathcal{Y}_t\right] + \\ &\quad \alpha_2(w)^2 E\left[W_{t-2}(w)^2 \mid \mathcal{Y}_t\right] + 2\; h_t(w) \alpha_1(w) E\left[W_{t-1}(w) \mid \mathcal{Y}_t\right] + \\ &\quad 2\; h_t(w) \alpha_2(w) E\left[W_{t-2}(w) \mid \mathcal{Y}_t\right] + h_t(w)^2. \end{aligned}$$

If we assume that $Y_t(w)|\ \mathcal{Y}_t$ is normally distributed, then K_{wt} is a linear combination of normals, so follows a normal distribution. Hence

$$\begin{aligned} E\left[K_{wt}^3|\ \mathcal{Y}_t\right] &= 3\left(E\left[K_{wt}^2|\ \mathcal{Y}_t\right] - E\left[K_{wt}|\ \mathcal{Y}_t\right]^2\right) E\left[K_{wt}|\ \mathcal{Y}_t\right] + E\left[K_{wt}|\ \mathcal{Y}_t\right]^3 \\ E\left[K_{wt}^4|\ \mathcal{Y}_t\right] &= 3\left(E\left[K_{wt}^2|\ \mathcal{Y}_t\right] - E\left[K_{wt}|\ \mathcal{Y}_t\right]^2\right)^2 + \\ &\quad 6\left(E\left[K_{wt}^2|\ \mathcal{Y}_t\right] - E\left[K_{wt}|\ \mathcal{Y}_t\right]^2\right) E\left[K_{wt}|\ \mathcal{Y}_t\right]^2 + E\left[K_{wt}|\ \mathcal{Y}_t\right]^4. \end{aligned}$$

Now

$$\begin{aligned} & E\left[K_{wt}K_{ut}|\ \mathcal{Y}_t\right] \\ &= E\left[(\ \alpha_1(w)W_{t-1}(w) + \ \alpha_2(w)W_{t-2}(w) + h_t(w))\right. \\ &\qquad \left.(\ \alpha_1(u)W_{t-1}(u) + \ \alpha_2(u)W_{t-2}(u) + h_t(u))|\ \mathcal{Y}_t\right] \\ &= \alpha_1(w)\ \alpha_1(u)E\left[W_{t-1}(w)W_{t-1}(u)|\ \mathcal{Y}_t\right] + \ \alpha_2(w)\ \alpha_1(u)E\left[W_{t-2}(w)W_{t-1}(u)|\ \mathcal{Y}_t\right] + \\ &\quad h_t(w)\ \alpha_1(u)E\left[W_{t-1}(u)|\ \mathcal{Y}_t\right] + \ \alpha_1(w)\ \alpha_2(u)E\left[W_{t-1}(w)W_{t-2}(u)|\ \mathcal{Y}_t\right] + \\ &\quad \alpha_2(w)\ \alpha_2(u)E\left[W_{t-2}(w)W_{t-2}(u)|\ \mathcal{Y}_t\right] + h_t(w)\ \alpha_2(u)E\left[W_{t-2}(u)|\ \mathcal{Y}_t\right] + \\ &\quad \alpha_1(w)h_t(u)E\left[W_{t-1}(w)|\ \mathcal{Y}_t\right] + \ \alpha_2(w)h_t(u)E\left[W_{t-2}(w)|\ \mathcal{Y}_t\right] + h_t(w)h_t(u). \end{aligned}$$

By bivariate normal distribution theory,

$$E\left[\left(K_{wt} - E\left[K_{wt}|\ \mathcal{Y}_t\right]\right)^2\left(K_{ut} - E\left[K_{ut}|\ \mathcal{Y}_t\right]\right)|\ \mathcal{Y}_t\right] = 0,$$

and

$$\begin{aligned} & E\left[\left(K_{wt} - E\left[K_{wt}|\ \mathcal{Y}_t\right]\right)^2\left(K_{ut} - E\left[K_{ut}|\ \mathcal{Y}_t\right]\right)^2|\ \mathcal{Y}_t\right] \\ &= \left(\mathrm{Var}\left(K_{wt}|\ \mathcal{Y}_t\right)\mathrm{Var}\left(K_{ut}|\ \mathcal{Y}_t\right) + 2\mathrm{Cov}\left(K_{wt}, K_{ut}|\ \mathcal{Y}_t\right)^2\right). \end{aligned}$$

Hence

$$
\begin{aligned}
& E\left[K_{wt}^2 K_{ut} |\ \mathcal{Y}_t\right] \\
&= 2E\left[K_{wt} |\ \mathcal{Y}_t\right] E\left[K_{wt}K_{ut} |\ \mathcal{Y}_t\right] - 2E\left[K_{wt} |\ \mathcal{Y}_t\right]^2 E\left[K_{ut} |\ \mathcal{Y}_t\right] + E\left[K_{wt}^2 |\ \mathcal{Y}_t\right] E\left[K_{ut} |\ \mathcal{Y}_t\right],
\end{aligned}
$$

$$
\begin{aligned}
& E\left[K_{wt}^2 K_{ut}^2 |\ \mathcal{Y}_t\right] \\
&= \left(\mathrm{Var}\left(K_{wt} |\ \mathcal{Y}_t\right) \mathrm{Var}\left(K_{ut} |\ \mathcal{Y}_t\right) + 2\mathrm{Cov}\left(K_{wt}, K_{ut} |\ \mathcal{Y}_t\right)^2\right) \\
&\quad + 2E\left[K_{wt} |\ \mathcal{Y}_t\right] E\left[K_{wt}K_{ut}^2 |\ \mathcal{Y}_t\right] - E\left[K_{wt} |\ \mathcal{Y}_t\right]^2 E\left[K_{ut}^2 |\ \mathcal{Y}_t\right] \\
&\quad + 2E\left[K_{ut} |\ \mathcal{Y}_t\right] E\left[K_{wt}^2 K_{ut} |\ \mathcal{Y}_t\right] - 4E\left[K_{wt}K_{ut} |\ \mathcal{Y}_t\right] E\left[K_{wt} |\ \mathcal{Y}_t\right] E\left[K_{ut} |\ \mathcal{Y}_t\right] \\
&\quad + 3E\left[K_{wt} |\ \mathcal{Y}_t\right]^2 E\left[K_{ut} |\ \mathcal{Y}_t\right]^2 - E\left[K_{wt}^2 |\ \mathcal{Y}_t\right] E\left[K_{ut} |\ \mathcal{Y}_t\right]^2.
\end{aligned}
$$

Moments of $W_t(w)$ are contained in the expressions of moments of K_{wt}. Note that

$$
\begin{aligned}
& E\left[W_t(w) |\ \mathcal{Y}_t\right] \\
&= \alpha_1(w) E\left[W_{t-1}(w) |\ \mathcal{Y}_t\right] + \alpha_2(w) E\left[W_{t-2}(w) |\ \mathcal{Y}_t\right] + E\left[Y_t(w) |\ \mathcal{Y}_t\right] \qquad (11)
\end{aligned}
$$

$$
\begin{aligned}
& E\left[W_t(w)W_t(u) |\ \mathcal{Y}_t\right] \\
&= E\left[\left(\alpha_1(w)W_{t-1}(w) + \alpha_2(w)W_{t-2}(w) + Y_t(w)\right) W_t(u) |\ \mathcal{Y}_t\right] \\
&= \alpha_1(w) E\left[W_{t-1}(w)W_t(u) |\ \mathcal{Y}_t\right] + \alpha_2(w) E\left[W_{t-2}(w)W_t(u) |\ \mathcal{Y}_t\right] + \\
&\quad E\left[Y_t(w)W_t(u) |\ \mathcal{Y}_t\right], \qquad (12)
\end{aligned}
$$

$$
E\left[W_t(w)W_{t-1}(u) |\ \mathcal{Y}_t\right]
$$

$$= \quad \alpha_1(w)E\left[W_{t-1}(w)W_{t-1}(u)\right|\ \mathcal{Y}_t] + \ \alpha_2(w)E\left[W_{t-2}(w)W_{t-1}(u)\right|\ \mathcal{Y}_t] +$$

$$E\left[Y_t(w)\right|\ \mathcal{Y}_t]\, E\left[W_{t-1}(u)\right|\ \mathcal{Y}_t],$$

$$E\left[W_{t-2}(w)W_t(u)\right|\ \mathcal{Y}_t]$$

$$= \quad \alpha_1(u)E\left[W_{t-2}(w)W_{t-1}(u)\right|\ \mathcal{Y}_t] + \ \alpha_2(u)E\left[W_{t-2}(w)W_{t-2}(u)\right|\ \mathcal{Y}_t] +$$

$$E\left[W_{t-2}(w)\right|\ \mathcal{Y}_t]\, E\left[Y_t(u)\right|\ \mathcal{Y}_t],$$

$$E\left[Y_t(w)W_t(u)\right|\ \mathcal{Y}_t]$$

$$= \quad \alpha_1(u)E\left[Y_t(w)\right|\ \mathcal{Y}_t]\, E\left[W_{t-1}(u)\right|\ \mathcal{Y}_t] +$$

$$\alpha_2(u)E\left[Y_t(w)\right|\ \mathcal{Y}_t]\, E\left[W_{t-2}(u)\right|\ \mathcal{Y}_t] + E\left[Y_t(w)Y_t(u)\right|\ \mathcal{Y}_t].$$

B Appendix: Forward recursion

The estimation procedure is recursive, starting at $t = 3$, and progressing iteratively forward in time. The values of $E\left[W_{3-l_1}(w)\right|\ \mathcal{Y}_t]$ and $E\left[W_{3-l_1}(w)W_{3-l_2}(u)\right|\ \mathcal{Y}_t]$ are initialized to an arbitrary value (positive for conditional expectation of squares) for all pairs of grid points u and w (including $u = w$) and $l_1 = 1, 2$; $l_2 = 1, 2$. At each time point t, we estimate the moments of Appendix A based on moments estimated at previous time points and on observations from time t.

Due to the forward recursive nature of the algorithm, rounding errors were occasionally compounded over time, especially when estimating at locations far from monitoring sites.

We discovered that the estimates based on (12) expanding $W_t(w)$ in terms of the AR(2) process, occasionally diverged from the similar expression expanding $W_t(u)$ as the AR(2) process (i.e., switching u and w in the right hand side of the equation). The values were identical to 8 decimal places for the first few iterations forward in time, but after a while there was a small discrepancy in the last decimal place, which compounded over time leading to instability of the estimation and variances occasionally growing to $\pm\infty$ over time. In order to avoid this, we now average the estimates based on expanding in the two ways at each iteration, and use this average value in the forward recursion. Errors of a smaller magnitude are more difficult to detect, but may still be compounded forward in time. Further investigation of this is needed.

References

[1] Akima, H. (1978) A method of bivariate interpolation and smooth surface fitting for irregularly distributed data points. *ACM Transactions on Mathematical Software*, **4**, 148-164.

[2] Blumenthal, D.L. (1993) Field Program Plan for the San Joaquin Valley Air Quality Study (SJVAQS) and the Atmospheric Utility Signatures, Predictions, and Experiments (AUSPEX) Program. Version 3, Post-Field Revision. *Report by Sonoma Technology, Inc. for the Valley Air Pollution Study Agency*, STI-98020-1241-FR.

[3] Box, G.E.P., Jenkins, G.M., and Reinsel, G.C. (1994) *Time series analysis : forecasting and control*. Third Edition. Prentice Hall.

[4] Brown, P.J., Le, N.D., and Zidek, J.V. (1994) Multivariate spatial interpolation and exposure to air pollutants. *The Canadian Journal of Statistics*, **22**, 489-509.

[5] Carroll, R.J., Chen, R., Li, T.H., Newton, H.J., Schmiediche, H., Wang, N., and George, E.I. (1997) Trends in ozone exposure in Harris County, Texas. *Journal of the American Statistical Association*, **92**, 392-415 (with discussion).

[6] Casado, L.S., Rouhani, S., Cardelino, C.A., and Ferrier, A.J. (1994) Geostatistical analysis and visualization of hourly ozone data. *Atmospheric Environment*, **28**: 2105-2118.

[7] Cressie, N.A.C. (1991) *Statistics for Spatial Data.* Wiley-Interscience. John Wiley and Sons, Inc.

[8] Guttorp, P., Le, N.D., Sampson, P.D., and Zidek, J.V. (1993a) Using entropy in the redesign of an environmental monitoring network. In *Multivariate Environmental Statistics*, G.P. Patil and C.R. Rao (eds), Elsevier Science Publishers, pp. 175-202.

[9] Guttorp, P., Meiring, W., Newman, K., and Sampson, P.D. (1993b) A space-time model for acidic precipitation. Poster presentation at Joint Statistics Meetings, San Francisco.

[10] Guttorp, P., Meiring, W., and Sampson, P.D. (1994) A space-time analysis of ground-level ozone data. *Environmetrics* **5**, 241-254.

[11] Guttorp, P., Meiring, W., and Sampson, P.D. (1997) Contribution to discussion of R.J. Carroll, R. Chen, T.H. Li, H.J. Newton, H. Schmiediche, N. Wang and E.I. George

(1997): Trends in ozone exposure in Harris County, Texas. *Journal of the American Statistical Association*, **92**: 405-408.

[12] Guttorp, P., and Sampson, P.D. (1994) Methods for Estimating Heterogeneous Spatial Covariance Functions with Environmental Applications. In *Handbook of Statistics XII: Environmental Statistics*, G.P. Patil, and C.R. Rao (eds), Elsevier/North Holland, New York. pp. 663-690.

[13] Høst, G., Omre, H., and Switzer, P. (1995) Spatial interpolation errors for monitoring data. *Journal of the American Statistical Association*, **90**, 853-861.

[14] Huang, H.-C., and Cressie, N.A.C. (1996) Spatio-temporal prediction of snow water equivalent using the Kalman filter. *Computational Statistics and Data Analysis*, **22**, 159-175.

[15] Jones, R.H. (1980) Maximum Likelihood Fitting of ARMA Models to Time Series With Missing Observations. *Technometrics*, **22**, 389-395.

[16] Journel, A.G., and Huijbregts, C.J. (1978) *Mining Geostatistics.* Academic Press, New York.

[17] Kendall, M., and Ord, J.K. (1990) *Time Series.* Oxford University Press.

[18] Meiring, W. (1995) *Estimation of Heterogeneous Space-Time Covariance.* Ph.D. Thesis, University of Washington.

[19] Meiring, W., Monestiez, P., Sampson, P.D., and Guttorp, P. (1997) Developments in the modelling of nonstationary spatial covariance structure from space-time monitoring data. In *Geostatistics Wollongong '96*, vol.1, E.Y. Baafi and N. Schofield (eds), Kluwer Academic Publishers, pp. 162-173.

[20] National Research Council (1991) *Rethinking the Ozone Problem in Urban and Regional Air Pollution.* National Academy Press, Washington, D.C.

[21] Sampson, P.D., and Guttorp, P. (1992) Nonparametric estimation of nonstationary spatial covariance structure. *Journal of the American Statistical Association*, **87**, 108-119.

[22] Sampson, P.D., Guttorp, P., and Meiring, W. (1994) Spatio-temporal analysis of regional ozone data for operational evaluation of an air quality model. *1994 Proceedings of the Section on Statistics and the Environment, American Statistical Association.* Alexandria: American Statistical Association, 46-55.

[23] Smith, T.B. (1994) Ozone Episode Forecasting in the San Joaquin Valley. In *Planning and Managing Air Quality Modeling and Measurement Studies: a Perspective through SJVAQS/AUSPEX*, P.A. Solomon and T.A. Silver (eds), Lewis Publishers/Pacific Gas and Electric Company, Chelsea, MI., pp. 507-527.

[24] Solomon, P.A., and Silver, T.A. (eds) (1994) *Planning and Managing Air Quality Modeling and Measurement Studies: a Perspective through SJVAQS/AUSPEX.* Lewis Publishers/Pacific Gas and Electric Company, Chelsea, MI.

[25] Statistical Sciences Inc. (1991) Splus Reference Manual, Vol. 1.

[26] Tiao, G.C., and Grupe, M.R. (1980) Hidden periodic autoregressive-moving average models in time series data. *Biometrika* **67**, 365-373.

[27] Wikle, C.K., and Cressie, N.A.C. (1996) A spatially descriptive, temporally dynamic statistical model with applications to atmospheric processes, pp. 118-182. In *"Spatio-temporal statistical models with applications to atmospheric processes"*, Ph.D. dissertation by C.K. Wikle, Dept. of Statistics, Dept. of Geological and Atmospheric Sciences, Iowa State University, Ames, IA.

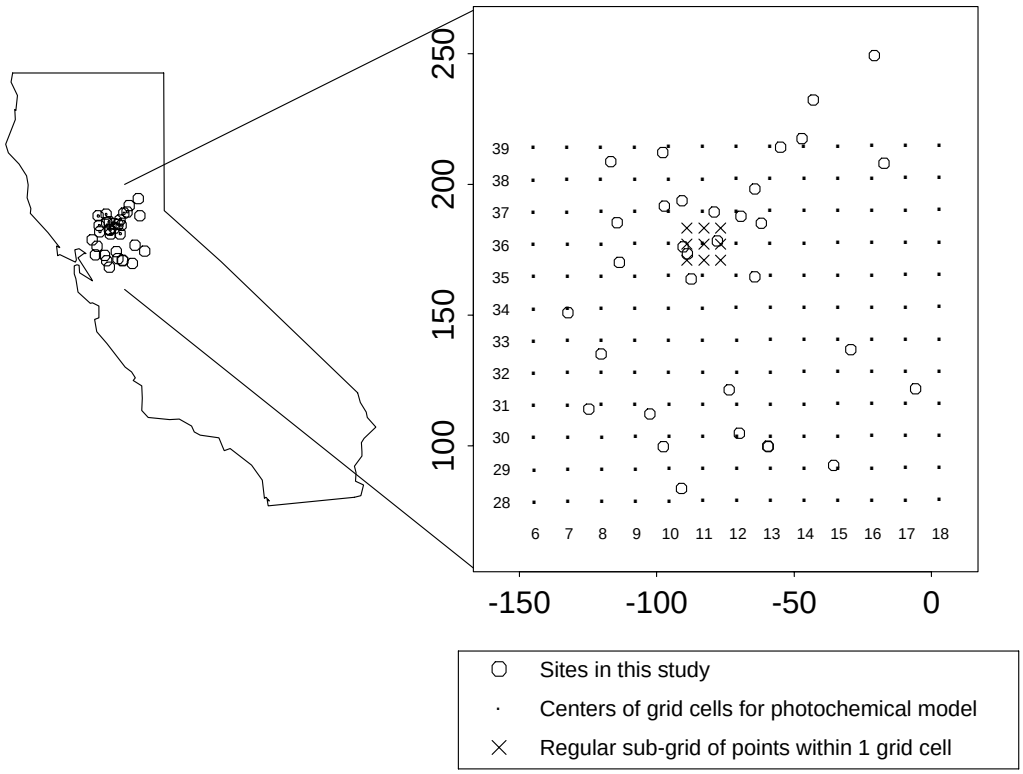

Figure 1: The locations of the 32 sites used in this study are indicated by open circles on the map of California, and again in an enlargement of the region containing the 32 sites. In the right subpanel, the centers of the grid cells corresponding to the SARMAP model results are indicated by dots. The crosses indicate a regular sub-grid of points in one of these grid cells. Similar sub-grids of points will be used for estimation of grid cell ozone levels for each grid cell of the geophysical model in this region, based on monitoring site observations. Locations are given in Lambert coordinates in the enlargement. The numbers along the margins indicate the model indices for the SARMAP model grid cells.

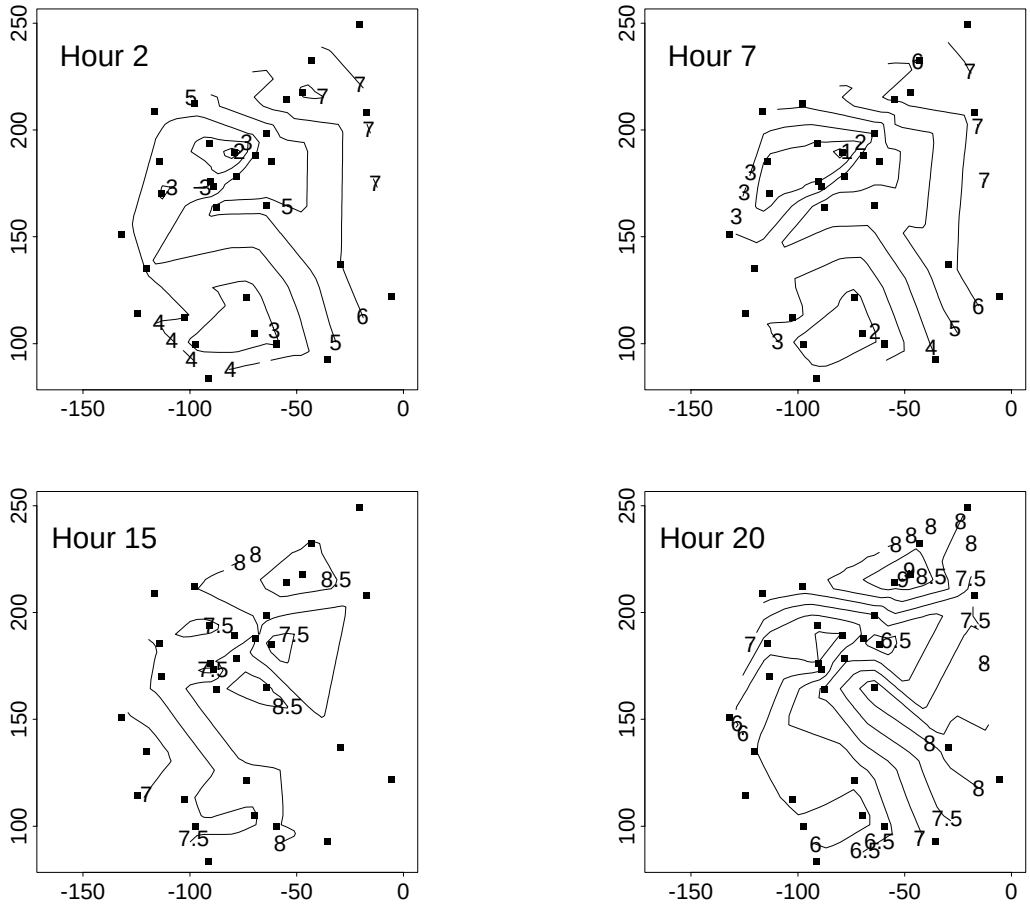

Figure 2: Contour plots of hourly means on the square root scale for four hours of the day, as indicated in the top left of each plot. The axes are in Lambert coordinates. Monitoring site locations are indicated by solid squares.

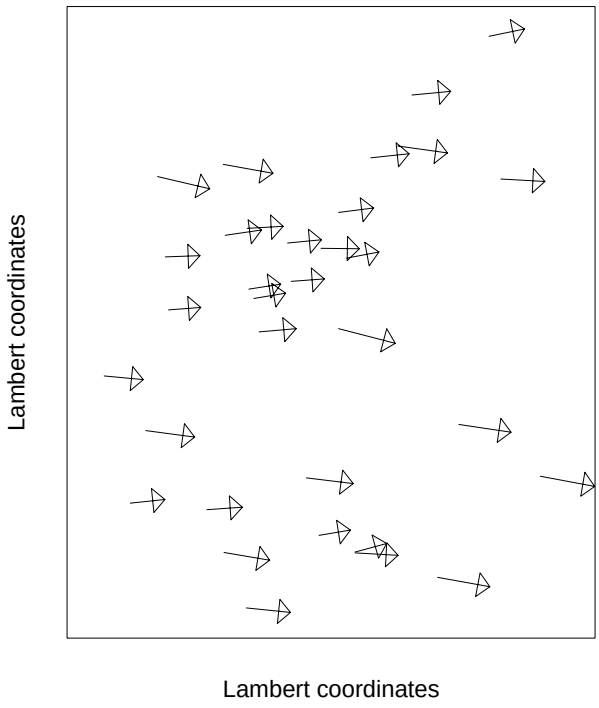

Figure 3: Relative magnitudes of site-specific AR(2) coefficients. An arrow originates at each site. The horizontal length of each arrow is proportional to the magnitude of the lag 1 coefficient in the AR(2) filter, while the vertical length is proportional to the magnitude of the lag 2 coefficient. The lag 1 coefficients range from 0.67 to 1.22, and the lag 2 coefficients range from -0.32 to 0.19.

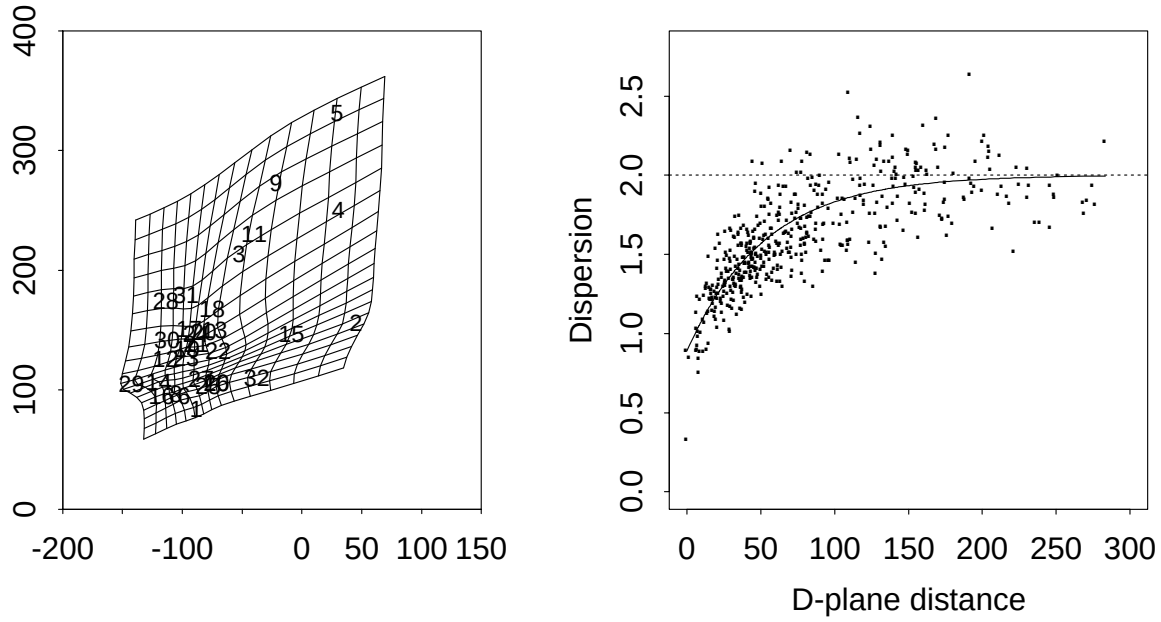

Figure 4: Deformation mapping and fitted variogram as a function of D-plane distance for hour 16.

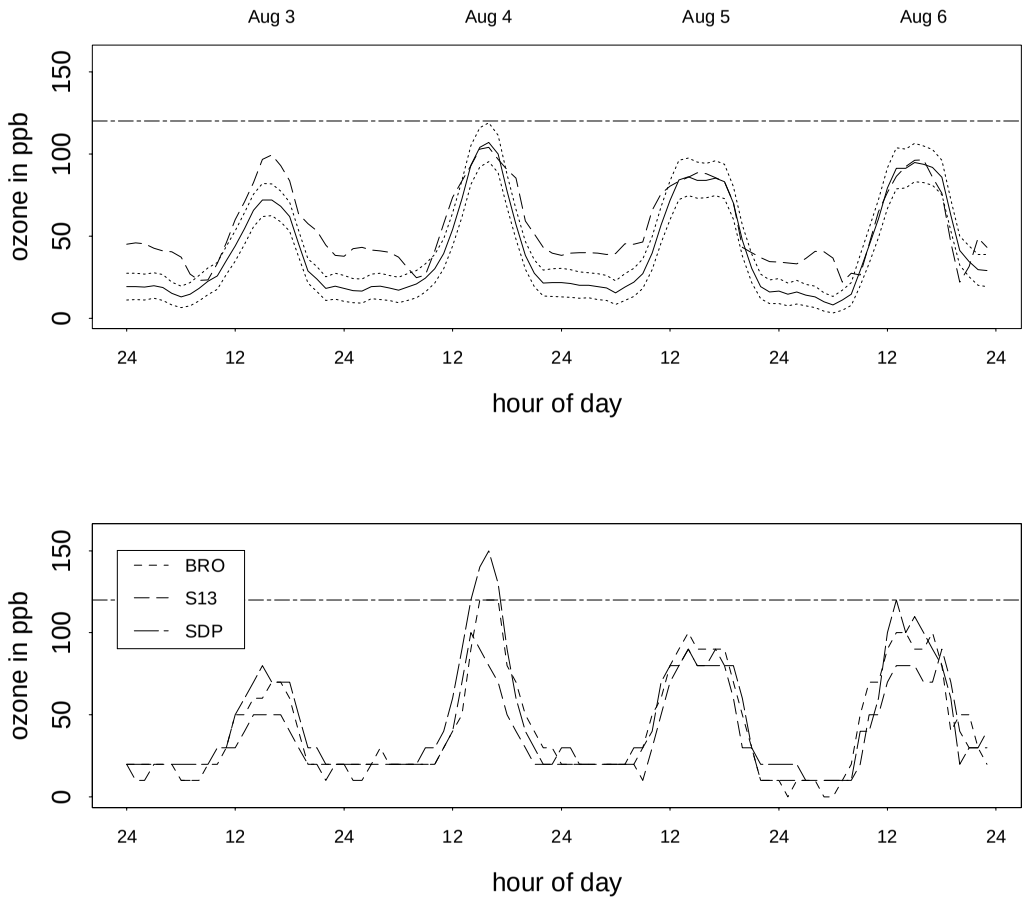

Figure 5: Comparison of model output and estimate of ozone concentration for one grid cell for the 4 days where model output was available. The solid line in the top figure represents the estimated ozone level for one grid cell in the Sacramento region. The dotted lines above and below the solid line show the areal estimate $\pm$ two standard errors. The broken line shows the model output. The lower plot shows time series of the observed ozone at three monitoring sites: BRO, S13 and SDP. These are the three sites that are partially covered by the crosses in Figure 1. Site descriptions are provided in Guttorp et al. (1994). The horizontal line in each of the panels indicates 120 ppb.

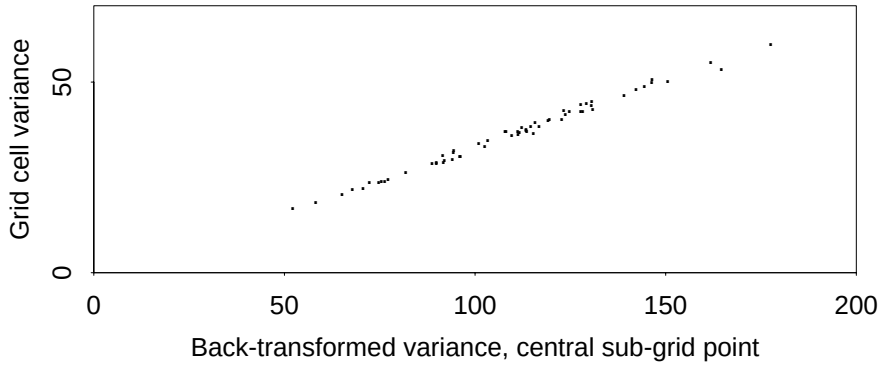

Figure 6: The estimated variances on the original ppb scale (equation 6) for the estimated grid cell ozone levels for one grid cell ($i = 11$, $j = 36$) at hour 16 are plotted against the corresponding variances of the point estimates in ppb at the central sub-grid point in this grid cell (one term in the first summation of the right hand of equation 6). Each point corresponds to a day during July or August 1990.

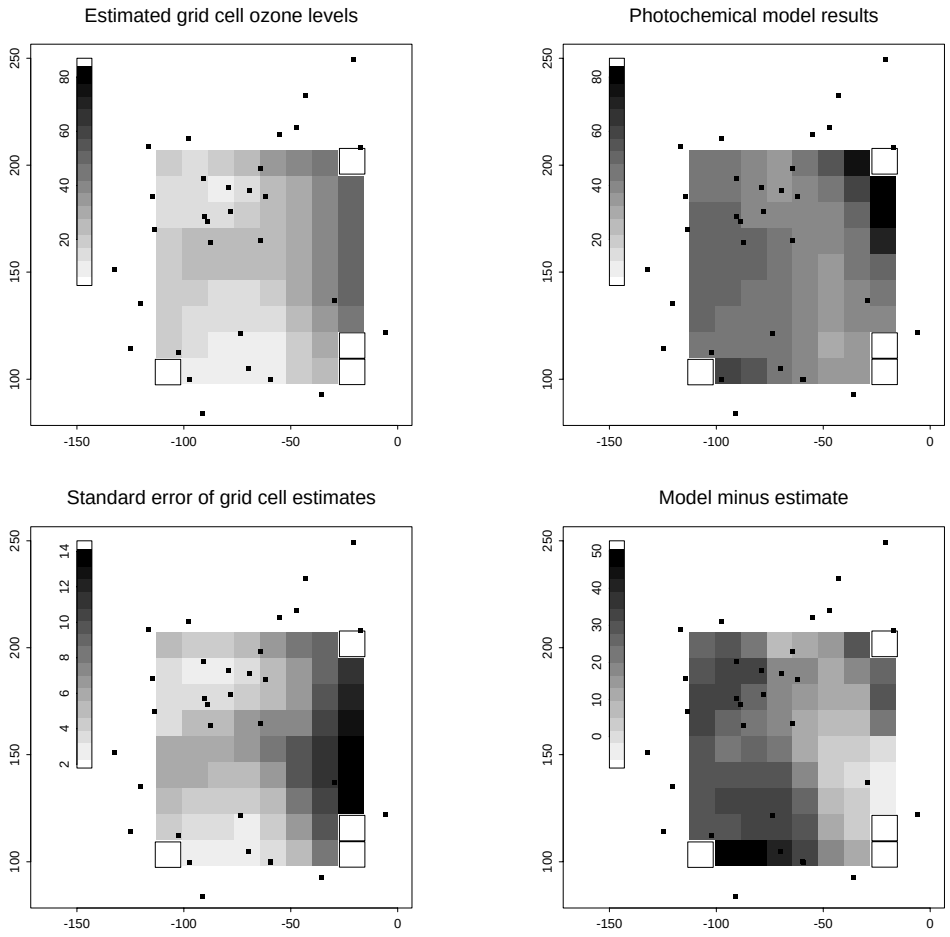

Figure 7: Image plots for hour 2 of August 4, 1990, showing the estimated grid cell averages (top left), the standard error estimates for the estimated grid cell averages (lower left), the model results for the grid cells (top right), and the model results minus the estimated grid cell ozone levels (lower right). Monitoring site locations are indicated by dots. We did not estimate for four grid cells, indicated by white outlined squares, due to problems extrapolating outside the convex hull of the monitoring sites. The axis increments are in kilometres derived from Lambert coordinate projections of latitude and longitude.

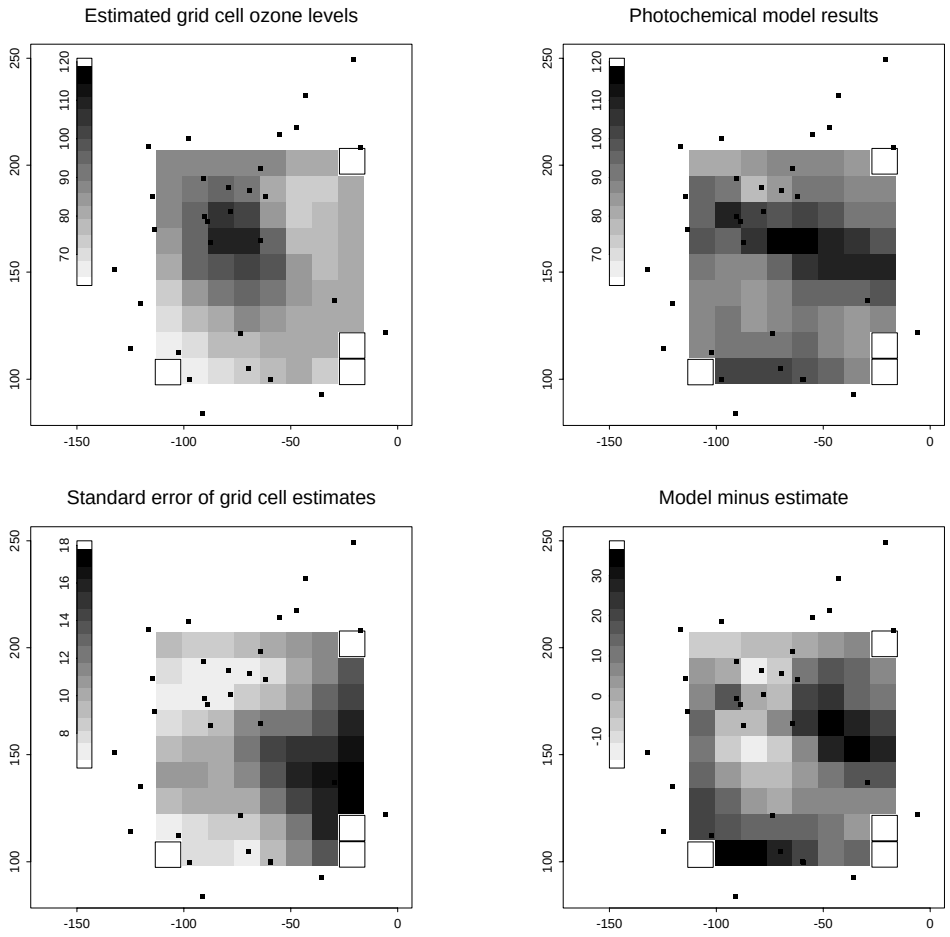

Figure 8: Image plots for hour 16 of August 4, 1990, showing the estimated grid cell averages (top left), the standard error estimates for the estimated grid cell averages (lower left), the model results for the grid cells (top right), and the model results minus the estimated grid cell ozone levels (lower right). Monitoring site locations are indicated by dots. We did not estimate for four grid cells, indicated by white outlined squares, due to problems extrapolating outside the convex hull of the monitoring sites. The axis increments are in kilometres derived from Lambert coordinate projections of latitude and longitude.